Journal of Materials Chemistry C

Accepted Manuscript

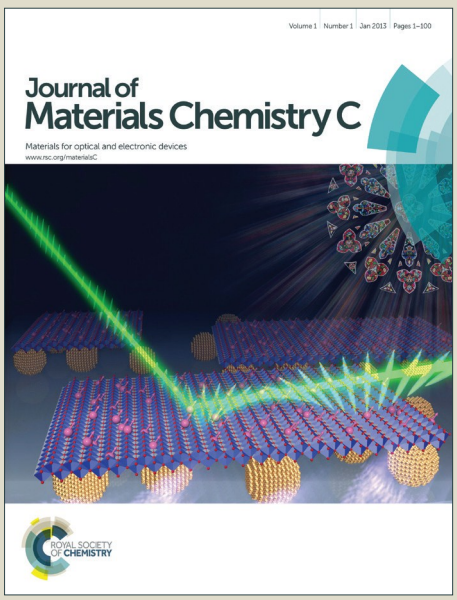

ROYAL SOCIETY OF CHEMISTRY

www.rsc.org/materialsC

Journal Name

RSCPublishing

ARTICLE

Benzothiazole-enamide-based BF_2 Complexes: Luminophores Exhibiting Aggregation-induced Emission, Tunable Emission and High Efficient Solid-State Emission

Cite this: DOI: Borebt10.Borebt10Borebt39/x0xx00000x

Received 00th January 2012,
Accepted 00th January 2012

DOI: 10.1039/x0xx00000x

www.rsc.org/

Qingsong Liu,[a] Xiaoqing Wang,*[,a] Hui Yan,[b] Yanping Wu,[a] Zhenyu Li,[a] Shuwen Gong,*[,a] Peng Liu[c] and Zhipeng Liu*[,a]

A series of benzothiazole-enamide-based boron difluoride complexes (**Borebt1–6**) were synthesized and characterized. These new luminophores were demonstrated to possess aggregation-induced emission, tunable, substituent-dependent emission profiles and large Stokes shift in solution. At the solid state, **Borebt1–6** exhibited intense emission with high quantum yield of 0.21–0.37. The photophysical properties and AIE characteristics of these compounds were rationalized through X-ray crystal analysis, electrochemical studies and theoretical calculations. Furthermore, **Borebt3–6** were capable of sensing of acidic gas by reversible changes of emission, which may potentially serve as solid-state fluorescent sensors for acidic vapors.

Introduction

Solid-state emissive organic luminophores have been intensively studied because of their potential applications in opto-electronic devices such as organic light-emitting diodes (OLEDs), fluorescent polarizers and sensors.[1] Organic difluoride boron complexes (BF_2 dyes), with 4,4'-difluoro-4-bora-3a,4a-diaza-s-indacene (**BODIPY**) as an example, are a family of well-known luminescent compounds, which display some excellent properties such as high molar absorption coefficients, outstanding fluorescence quantum yields and tunable emission from visible light to near infrared.[2] However, despite their intense fluorescence in solution, BF_2 dyes show very weak emission in their aggregated states, and this "aggregation-caused emission quenching (ACQ)" has greatly limited the practical applications of BF_2 dyes as electroluminescence materials.[2c, 3] Thus, great efforts have been paid to the design and synthesis of new BF_2 luminophores, in particular, based on novel frameworks, with high emission in the solid state.

The ACQ of BF_2 dyes is caused by self-absorption resulting from their narrow Stokes shifts and aggregation-induced energy transfer. The narrow Stokes shifts (typically 200-400 cm^{-1}) of BF_2 dyes are attributed to their rigid symmetrical molecular structures with minimal difference between the ground- and excited-states.[2] On the other hand, BF_2 dyes with panel-like structure often exhibit strong intermolecular interactions (e.g., π–π stacking, the formation of excimers and exciplexes) in their aggregation states, which quenches the emission efficiency. Various strategies have been developed to construction of solid-state emissive BF_2 dyes via the way of improve the Stokes shift and/or decrease intermolecular interactions of BF_2 dyes. Desymmetrization of the *N*,*N*-bidentate ligand of BF_2 dyes and decorating BF_2 dyes with bulky groups have been proved to be effective strategies for decreasing intermolecular aggregation.[2,4,5] Nevertheless, aggregation-induced emission (AIE) which was discovered by Tang et al can also be a useful strategy for the development of fluorescent luminophores with high emission in the solid state.[6] However, only few examples of BF_2 luminophores with AIE have been developed due to the lack of appropriate frameworks.[7]

Recently, we have reported that boron complexes based on pyridyl-enamido-ligands with propeller-shape structure showed interesting fluorescence properties such as large Stokes shift, high solid-state emission and AIE effect.[7h] In light of this research, we can rationalized that design of boron complexes with propeller-shaped structure should be useful for the development of new AIE-active BF_2 complexes. In the course of our studies on the development of solid-state emissive boron complexes bearing heterocycle-enamido-ligand, we are interested in the synthesis of the BF_2 complex based on benzothiazole structure. In this paper, we report the synthesis and fluorescence properties of a series benzothiazole-enamide-based BF_2 complex (Fig. 1). **Borebt1–6** possess a general propeller-shaped non-planar molecular structure in the solid state and exhibit spectacular luminescence characteristics: AIE and tunable emission profiles in solution and high efficient solid-state emission.

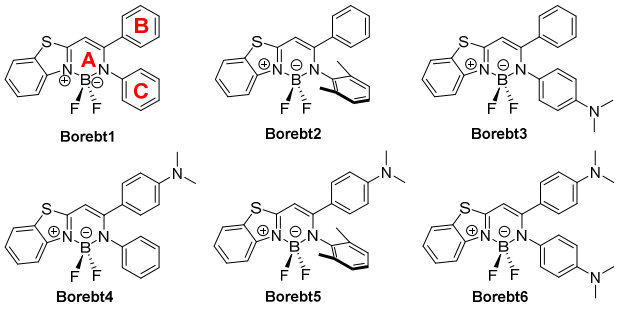

Fig. 1. Chemical structures of **Borebt1–6**.

Results and Discussion

Synthesis of Borebt1–6. **Borebt1–6** were synthesized from benzothiaole-enamide-based *N*,*N*-bidentate ligands (Scheme 1). The reaction of 2-methylbenzothiazole with ethyl benzoate or methyl 4-(dimethylamino)benzonate gave compounds **1** [7g] and **2**. **1** and **2** were reacted with aniline, 2,6-dimethylaniline and 4-(dimethylamino)aniline in the presence of CF_3COOH (cat.) in toluene to afford the benzothiaole-enamide-based *N*,*N*-bidentate ligands **3-8**. By reacting of **3-8** with boron trifluoride etherate in the presence of DBU in toluene gave **Borebt1–6** in high yield. The structures of compounds **Borebt1–6** were confirmed by ^1H, ^{11}B, ^{13}C NMR, ESI-MS, elementary analysis and X-ray crystallography.

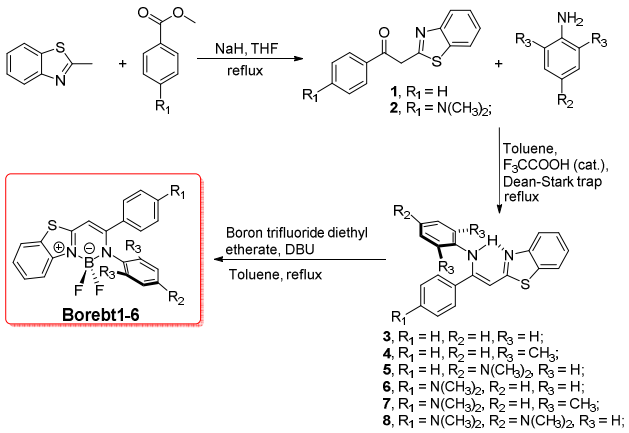

Scheme 1. Synthetic routes for compounds **Borebt1–6.**

General Optical Properties of Borebt1–6. The photophysical properties of **Borebt1–6** were measured in different solvents and in the solid state. The full details can be found in Fig. 2, S1–2 and Table 1. In THF, **Borebt1–3** showed absorption maxima at 392 nm (ε = 19000 $M^{-1}cm^{-1}$), 386 nm (ε = 40200 $M^{-1}cm^{-1}$) and 397 nm (ε = 19300 $M^{-1}cm^{-1}$), respectively. Compared with **Borebt1–3**, **Borebt4–6** showed red-shifted absorption bands (~15 nm) with absorption maxima at 409 nm (ε = 37700 $M^{-1}cm^{-1}$), 405 nm (ε = 39000 $M^{-1}cm^{-1}$) and 408 nm (ε = 35500 $M^{-1}cm^{-1}$), respectively. The red shift of absorption band can be explained by the *N*, *N*-dimethylamino group at B ring caused charge transfer (CT) enhancement. On the other hand, **Borebt1** and **Borebt3**, and **Borebt4** and **Borebt6** exhibited almost the same absorption maxima, suggesting that *N*,*N*-dimethylamino group in C ring has less electronic effect on the fundamental states of **Borebt1–6**. The solvent effects on the absorption of **Borebt1–6** were examined (Fig. S1). The absorption bands of **Borebt1–6** were hardly affected by solvent polarity.

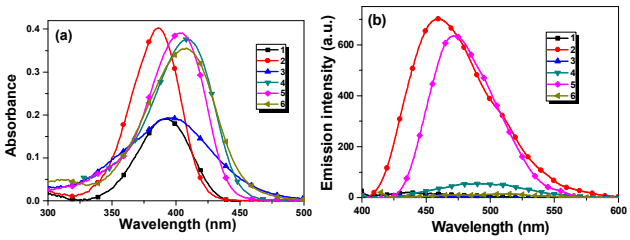

Fig. 2. Absorption (a) and Emission (b) spectra of **Borebt1–6** (10 μM) in THF.

Borebt1, **Borebt3**, **Borebt4** and **Borebt6** were found to possess broad fluorescence emission spectra spanning 400–600 nm, associated with very low fluorescence quantum yields in low-viscosity solvents. While in high-viscosity solvents such as glycerol, these compounds showed dramatically enhanced fluorescence intensity (Fig. 2b and S2). This result suggests that the viscous medium inhibits intramolecular rotation, thereby suppressing the nonradiative process which leads to increased Φ_f (Table 1). It should be noted that, **Borebt1** and **Borebt4** showed enhanced fluorescence intensity in glycol or glycerol, while the fluorescence intensity enhancement of **Borebt3** and **Borebt6** was only found in glycerol. This should be ascribed to the additional rotation group (*N*,*N*-dimethylamino group) of **Borebt3** and **Borebt6** induced more nonradiative process than **Borebt1** and **Borebt4**.[7h]

With two methyl groups in C ring, **Borebt2** and **Borebt5** showed relatively strong fluorescence in solution (Fig. 2b and S2), which suggests that the intramolecular rotation induced nonradiative process of **Borebt2** and **Borebt5** was inhibited efficiently. The maximum fluorescence wavelength (F_{max}) of **Borebt2** showed almost no variation with changing solvent polarity, and only an intensity change was observed in different solvents (Fig. S2b). **Borebt5** showed a red shift of the emission band and increment of the emission intensity with the increasing of the polarity of solvents. This should be ascribed to the *N*,*N*-dimethylamino group at B ring caused CT enhancement.[6] It should be noted that **Borebt5** showed slightly red-shifted emission (~6 nm) in glycerol when compared with **Borebt1–4**, which suggests that the ICT effect of the *N*,*N*-dimethylamino group at B ring was inhibited due to the steric effect of the two methyl groups in C ring (Fig. S2e).

In the solid state, **Borebt1–6** showed almost the same absorption maxima with λ_{abs} at 393 nm, 388 nm, 410 nm, 392 nm, 405 nm and 414 nm, respectively, compared with those in solution. The emission bands of **Borebt1–6** remained narrow and the F_{max} values (482–555 nm) were more bathochromic than those in THF (438–485 nm) (Fig. 3, S3 and Table 1). The red-shift of emission band should be ascribed to the aggregation-induced CT enhancement.[6,7]

Table 1. Photophysical data of **Borebt1–6** in solution and in the solid state.

Compound	In solution					In the solid state[f]		
	λ_{abs} (nm) ε (mol^{-1} cm^{-1}) THF [a]	λ_{em} (nm) (Φ_f) THF [a],[c]	λ_{em} (nm) (Φ_f) Aggr [b],[c]	λ_{em} (nm) (Φ_f) Glycerol [a], [c]	SS (cm^{-1}) [d]	λ_{abs} (nm)	λ_{em} (nm)	Φ_f [e]
Borebt1	392 (19000)	447 (0.01)	480 (0.07)	449 (0.10)	3140	393	494	0.29
Borebt2	386 (40200)	458 (0.17)	458 (0.11)	450 (0.34)	4070	388	482	0.37
Borebt3	397 (19300)	438 (0.03)	576 (0.16)	449 (0.20)	2360	410	547	0.27
Borebt4	409 (37700)	485 (0.01)	521 (0.07)	497 (0.14)	3830	392	506	0.21
Borebt5	405 (39000)	472 (0.37)	503 (0.53)	456 (0.38)	3500	405	508	0.30
Borebt6	408 (35500)	448 (0.02)	545 (0.20)	519 (0.25)	2190	414	555	0.23

[a] Measured at a concentration of 10 μM in THF or glycerol at 25 °C; [b] Measured at a concentration of 10 μM in THF/water at 25 °C; [c] Determined by using 4-methylamino-7-nitro-2,1,3-benzoxadiazole (Φ_f = 0.38 in acetonitrile) as reference; [d] Frequency units between the longest absorption band and emission band in THF; [e] Absolute quantum yield determined by calibrated integrating sphere systems; [f] Powder examples were used for the absorption and emission measurement.

Importantly, **Borebt1–6** showed intense emission in the solid state with high Φ_f of 0.29, 0.37, 0.27, 0.21, 0.30 and 0.23, respectively. This result suggests that the interactions of **Borebt1–6** should be very weak in the solid state, and AIE was at play in **Borebt1–6**.

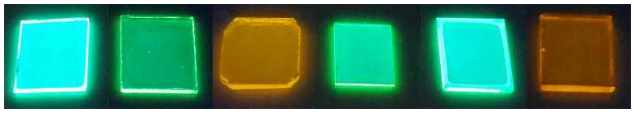

Fig.3. The photo picture of **Borebt1-6** (from left to right) in drop-cast film (λex = 365 nm using a UV lamp).

In order to confirm whether **Borebt1–6** have the AIE character, the emission properties of **Borebt1–6** were investigated in THF–water mixture of various ratios (Fig. 4,.S4 and Table 1). In pure THF, **Borebt1**, **Borebt3**, **Borebt4** and **Borebt6** had very low emission intensity. When water was added to the THF solution, the emission intensity of **Borebt1**, **Borebt3** and **Borebt6** kept almost the same until the water fraction (f_w) reached 80%, 80% and 70%, respectively. However, upon addition of 99% (for **Borebt1**), 99% (for **Borebt3**) and 80%(for **Borebt6**) water in THF, the emission intensity of **Borebt1**, **Borebt3** and **Borebt6** was significantly enhanced, and the Φ_f value was 0.07 for **Borebt1**, 0.16 for **Borebt3** and 0.20 for **Borebt6**, which was 7-fold, 5-fold and 10-fold higher than that in pure THF solution. Interestingly, **Borebt4** showed gradually increment of the emission intensity with the addition of water into THF solution. In contrast to **Borebt1**, **Borebt3**, **Borebt4** and **Borebt6**, **Borebt2** and **Borebt5** showed intense emission in THF solution with Φ_f of 0.17 and 0.37, respectively. With the addition of water, the emission of **Borebt2** slightly quenched with the increment of f_w, while the emission intensity of **Borebt5** increased in a small range (Fig. 4b, 4e). With the additional *N*,*N*-dimethylamino group in B and/or C phenyl rings, **Borebt3–6** showed large red-shifted emission with the increase of f_w, and this should be ascribed to the aggregation-induced CT enhancement (Fig. 4c-f).[6,7] The aqueous solution of **Borebt2** and **Borebt4-6** became turbid when the f_w exceeded 80%, 80%, 70% and 90%, respectively, because of the formation of visible aggregates that hindered the acquisition of the emission spectra. As mentioned above, the addition of water into the THF solutions of **Borebt1** and **Borebt3–6** resulted in aggregation that led to enhanced/red-shifted emission. The restriction of phenyl ring and *N*,*N*- dimethylamino group's free rotation via aggregates formation should be responsible for this AIE.[7]

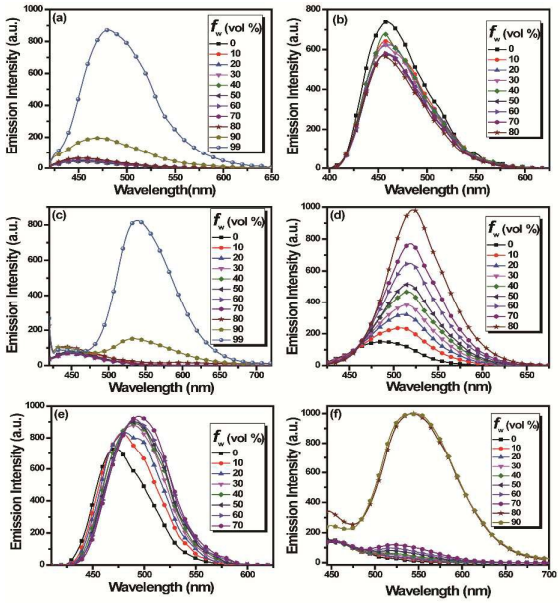

Fig. 4. Emission spectra of **Borebt1** (a), **Borebt2** (b), **Borebt3** (c), **Borebt4** (d), **Borebt5** (e) and **Borebt6** (f) in THF/water mixtures (10 μM) with varied volumetric fractions of water (f_w).

X-ray crystal structure analysis. In order to better understand the aggregation and solid-state emission properties of **Borebt1–6**, X–ray crystallographic analysis was performed. The ORTEP drawings and molecular packing structures of **Borebt1–6** are shown in Fig. 5 and Fig. S5. All the boron atoms of **Borebt1–6** adopt a typical tetrahedral geometry to form *N*^*N*–chelate six-membered rings (ring B), which contributes to the construction of the three-ring-fused π–conjugated skeletons. As anticipated, **Borebt1–6** adopt propeller-shaped conformations. The dihedral angles of A and B and A and C are 69.86° and 66.16° in **Borebt1**, 59.48° and 78.06° in **Borebt2**, 54.40° and 66.59° in **Borebt3**, 35.43° and 69.73° in **Borebt4**, 51.06° and 81.38° in **Borebt5**, 55.69° and 79.40° in **Borebt6**, respectively.

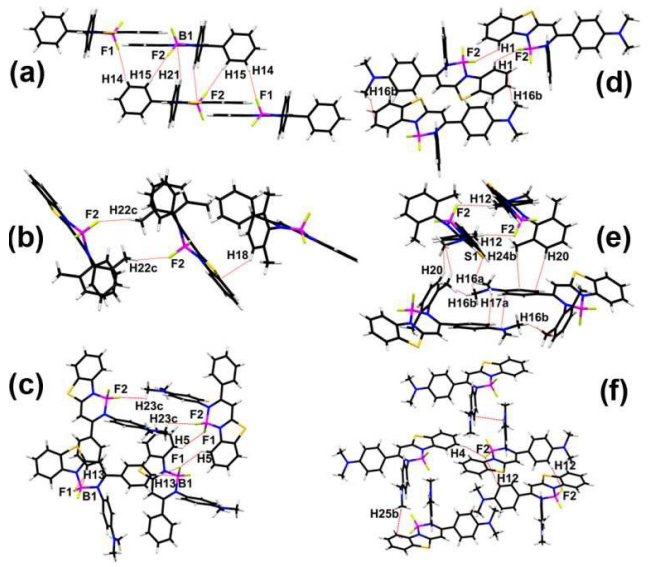

Fig. 5. Crystal packing structures of **Borebt1** (a), **Borebt2** (b), **Borebt3** (c), **Borebt4** (d), **Borebt5** (e) and **Borebt6** (f). The red dotted lines show intermolecular interactions within **Borebt1–6**.

Intermolecular π–π interactions were not detected in **Borebt1–6**. However, multiple short interatomic contacts existed within the crystals: F1···H14–C14 (135.98°, 3.34 Å), F2···H15–C15 (166.70°, 3.32 Å), and B1···H21–C21 (158.52°, 4.05 Å) interactions in **Borebt1**, F2···H22c–C22 (167.38°, 3.58 Å) interactions in **Borebt2**, F1···H5–C5 (132.72°, 3.25 Å), F1···H13–C13 (142.29°, 3.32 Å), F2···H23c–C23 (110.05°, 3.09 Å), and B1···H13–C13 (127.50°, 3.82 Å) interactions in **Borebt3**, F2···H1–C1 (127.19°, 3.08 Å) interactions in **Borebt4**, F2···H12–C12 (135.33°, 3.39 Å) and S1···H16a–C16 (149.92°, 3.75 Å) interactions in **Borebt5**, F2···H4–C4 (149.47°, 3.45 Å) and F2···H12–C12 (172.61°, 3.54 Å) interactions in **Borebt6**. Furthermore, C–H···π interactions were detected in **Borebt2** (3.56 Å), **Borebt3** (3.70 Å), **Borebt5** (3.6-3.9Å) and **Borebt6** (3.55 Å). These weak intermolecular interactions fix the molecular conformations of **Borebt1–6** in the solid state, thus inhibiting the internal rotations and blocking their non-radiative relaxation. These results agree well with the observation that **Borebt1–6** show intense emissions in the solid state.

Electrochemical studies. The electrochemical behaviors of **Borebt1–6** were investigated by cyclic voltammetry (CV) (Fig. 6). **Borebt1–6** have similar two couple of irreversible reduction peaks. The calculated LUMO levels of **Borebt1–6** are around -2.36~-2.67 eV (Fig. 6 and Table 2). **Borebt1** and **Borebt2** display one irreversible oxidation peak originated from the benzothiazole moiety, with high potential of 0.96 eV and 1.01 eV, respectively. For **Borebt4–5**, except for the oxidation peaks originated from the benzothiazole moiety, the irreversible peaks at 0.51 eV and 0.59 eV are attributed to the *N*,*N*-dimethylamino group in **B** phenyl ring. **Borebt3** and **Borebt6** with the *N*,*N*-dimethylamino group in **C** phenyl ring display three and four irreversible oxidation peaks, respectively. The HOMO energy levels for **Borebt1–6** are calculated to be -5.98 eV for **Borebt1**, -5.99 eV for **Borebt2**, -5.75 eV for **Borebt3**, -5.55 eV for **Borebt4**, -5.58 eV for **Borebt5**, and -5.60 eV for **Borebt6**, respectively (Fig. 6 and Table 2). Based on these results, we can conclude that the introduction of the electron-donating *N*,*N*-dimethylamino group only raises HOMO levels of **Borebt1–6**, while has less effect on LUMO levels, leading to a red shift in the absorption spectra.

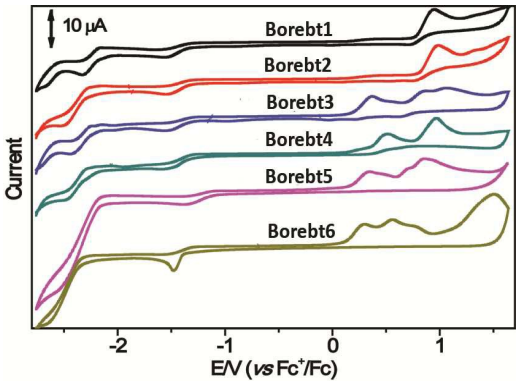

Fig. 6. Cyclic Voltammagrams of **Borebt1–6**. Samples run in CH_2Cl_2, 0.1 mM Bu_4NBF_4 electrolyte and scan rate at 50 mV s^{-1}.

Theoretical Calculations. To further illustrate the effect of the structure modification on the electronic structures which related to the photophysical properties of **Borebt1–6**, time-dependent density functions theory (TD-DFT) calculation was carried out using the crystal structures as model structures.[8] The pictorial drawings of HOMOs and LUMOs and energy levels are shown in Fig. 7, S6 and Table 2.

Borebt1 and **Borebt2** have HOMOs delocalized over the benzathiazole unit and the BF_2 core (A ring), whereas their LUMOs are mostly localized on the benzothiazole unit, A and B rings. The calculated first excited state, mainly consisting of HOMO→LUMO transition, have excitation energies of 3.64 eV (340 nm, f = 0.6729) for **Borebt1** and 3.58 eV (346 nm, f = 0.6343) for **Borebt2**, respectively. The incorporation of *N*,*N*-dimethyl group in **Borebt3** is predicated to greatly increase the HOMO energy level by 0.8 eV, but to have little effect on the LUMO, thus decreasing the HOMO-LUMO gap, and resulting in red shift of the main absorption band relative to those of **Borebt1** and **Borebt2**. The lowest-energy absorption band of **Borebt3** is dominated by excited state corresponding to the HOMO-1→LUMO transition (3.58 eV, 346 nm, f = 0.6135), but also contains a excited state with minor oscillation strength corresponding to the HOMO→LUMO transition (2.73 eV, 451 nm, f = 0.1130). The energy levels of HOMOs and LUMOs of **Borebt4–5** are both increased relative to those of **Borebt1–2**, due to the introduction of the electron donating amino substituent. The decreased HOMO-LUMO gaps of **Borebt4–5** should be responsible for the red-shifted main absorption band relative to those of **Borebt1** and **Borebt2**. **Borebt4–5** have HOMOs delocalized over the benzathiazole unit, A, B rings and the *N*,*N*-dimethyl group in B ring, whereas their LUMOs are mostly localized on the benzothiazole unit and A ring. The calculated first excited state of **Borebt4–5**, mainly consisting of

HOMO→LUMO transition, have excitation energies of 3.30 eV (375 nm, f = 0.9230) for **Borebt4** and 3.32 eV (372 nm, f = 0.7317) for **Borebt5,** respectively. **Borebt3** and **Borebt6,** which also have *N*,*N*-dimethyl group in C ring, show higher HOMO levels than **Borebt4** and **Borebt5**. **Borebt6** has HOMO delocalized over the benzathiazole unit, A, B rings and the *N*,*N*-dimethyl group in B ring, and HOMO-1 delocalized over the C ring. Its LUMO is mostly localized on the benzothiazole unit and A ring. The maximum absorption band of **Borebt6** is dominated by the excited state corresponding to the HOMO-1→LUMO transition (3.39 eV, 365 nm, f = 0.6676), and the first excited state dominated by HOMO→LUMO component has a relative weak oscillation strength (3.01 eV, 410 nm, f = 0.0183).

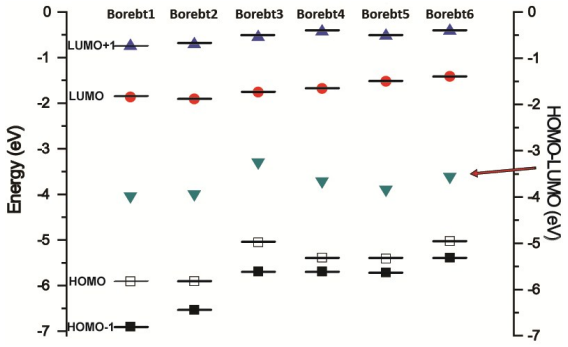

Fig. 7.The frontier MO energies and HOMO–LUMO gaps of **Borebt1–6**.

It is obvious that the lowest-energy excited state for all dyes corresponds to a charge transfer from the benzothiazole fragment and *N*,*N*-dimethyl group in the B and C rings to the A ring. The features of charge transfer make the ground and excited states more energetically distinct, leading to large Stokes shifts. These results indicate that the main absorption bands of **Borebt1–6** can be tuned by benzothiazole units and B and C rings with different substitute groups, and that the extent of shift of the absorption can be predicted by theoretical calculations.

Acidchromic properties in the solid state. Since the *N*,*N*-dimethylamino group in **Borebt3–6** can be easily protonated by acid, the applications of **Borebt3–6** as solid-state fluorescent sensors for acidic vapors were examined (Fig. 8 and S13–15). **Borebt3–6** emitted intense fluorescence in the powder solid state. When exposed to HCl vapors for a few seconds, **Borebt3** and **Borebt6** exhibited a blue-shift of emission with colour changing from yellow to cyan (547 nm to 518 nm) for **Borebt3**, and orange to yellowish green (555 nm to 504 nm) for **Borebt6**. In contrast, the fluorescence of **Borebt4–5** was effectively quenched after exposing to HCl vapors without the shift of emission. The blue-shift of the emission is due to the diminished CT. And the quenched emission is probably because of the changed molecular conformation and packing structure.[9] The protonated powder samples gradually recovered their original colour and fluorescence when they were treated with NH_3 vapor for few minutes. The switching between emission red-shift/turn-on and emission blue-shift/quenching states by HCl/NH_3 vapor fuming can be carried out repeatedly without obvious intensity decaying.

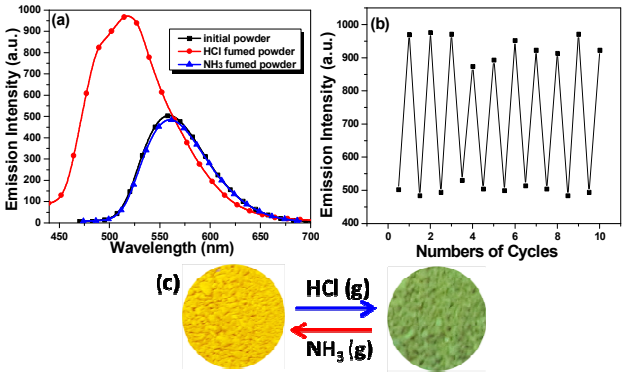

Fig. 8. (a) Emission spectra of initial, HCl (g) and NH_3 (g) fumed powders of **Borebt3**; (b) Reversible switching of the emission of **Borebt3** by HCl/NH_3 fuming cycle; (c) Fluorescent pictures of HCl (g) and NH_3 (g) fumed powders of **Borebt3**.

Table 2. HOMO, LUMO and HOMO-LUMO gaps of compounds **Borebt1–6**.

Compound	HOMO-1 (eV)[a]	HOMO (eV)[a]	LUMO (eV)[a]	LUMO+1 (eV)[a]	E_g (eV)[a]	HOMO (eV)[b]	LUMO (eV)[b]	E_g (eV)[c]
Borebt1	-6.89	-5.82	-1.84	-0.73	3.98	-5.98	-2.67	3.31
Borebt2	-6.53	-5.81	-1.88	-0.69	3.93	-5.99	-2.56	3.43
Borebt3	-5.69	-4.98	-1.73	-0.54	3.24	-5.75	-2.64	3.11
Borebt4	-5.69	-5.31	-1.65	-0.42	3.65	-5.55	-2.63	2.92
Borebt5	-5.71	-5.33	-1.49	-0.51	3.83	-5.58	-2.36	3.22
Borebt6	-5.38	-4.95	-1.39	-0.41	3.55	-5.60	-2.48	3.12

[a] HOMO, LUMO and band-gap (E_g) levels were calculated from the TD-DFT calculations. [b] HOMO and LUMO levels were determined from the onset of the first oxidation and reduction with reference to the HOMO of ferrocene (-4.8 eV), which was used as an internal standard; [c] E_g were obtained from the CV.

Conclusions

In this article, a new series of BF_2 luminophores (**Borebt1–6**) were developed by reacting of benzothiazole-enamide-based desymmetrized *N*,*N*-bidentate ligands with boron trifluoride etherate. The complexes were characterized by X-ray crystallography and NMR spectroscopy and their photophysical properties were investigated. Due to the intramolecular rotation induced nonradiative process, **Borebt1**, **Borebt3–4** and **Borebt6** exhibited AIE characteristics and fluorescence efficiently in the aggregate state. **Borebt2** and **Borebt5**, which have two methyl groups in C ring, showed relatively strong

fluorescence both in low- and high-viscosity organic solvents, suggesting the intramolecular rotation induced nonradiative process of **Borebt2** and **Borebt5** was inhibited efficiently. **Borebt1–6** exhibited intense emission in the solid state with high quantum yield of 0.21-0.37. X–ray crystallographic analysis demonstrated that the weak intermolecular interactions such as F···H–C and C–H···π by fixing the molecular conformations of **Borebt1–6** were responsible for intense fluorescence in the solid state. The theoretical calculation and electrochemical studies suggested that the incorporation of *N*,*N*-dimethylamino group into the phenyl rings raised HOMO levels of **Borebt3–6**, while had less effect on LUMO levels. Furthermore, due to the Lewis-base nature of *N*,*N*-dimethylamino group, **Borebt3–6** were capable of sensing of acidic gas by reversible changes of emission, which may potentially serve as solid-state fluorescent sensors for acidic vapors.

Experimental Section

Spectroscopic measurements

UV-vis absorption spectra were recorded on a Shimadzu UV-3600 spectrometer with a resolution of 1.0 nm. A solution of the sample (ca. 10^{-5} M) in a 1 cm square quarts cell was used for the measurement. Fluorescence spectra were recorded on a Hitachi F-7000 spectrometer. The fluorescence lifetimes and the absolute quantum yields (Φ_f) of the samples were determined with a Horiba Jobin Yvon Fluorolog-3 spectrofluorimeter. Fluorescence quantum yield of **Borebt1–6** in solution were determined by using 4-methylamino-7-nitro-2,1,3-benzoxadiazole (Φ_f = 0.38 in acetonitrile) as reference.[10]

X-ray structure determination

The X-ray diffraction data were collected at 298 K on a Gemini A Single Crystal CCD X-ray diffractometer with $Mo_{K\alpha}$ radiation (l = 0.71073 Å) and graphite monochromator. The structure was solved by direct methods (SHELX-97)[11] and refined by the full-matrix least-squares on F_2 (SHELX-97). All the non-hydrogen atoms were refined anisotropically and all the hydrogen atoms were placed by using AFIX instructions.

Borebt1: $C_{21}H_{15}BF_2N_2S$; Triclinic, P-1, a = 9.1766(9) Å, b = 9.2490(10) Å, c = 11.8304(13) Å, α = 109.989(10)°, β = 96.898(9)°, γ = 99.154(9)°, V = 914.97(17) Å^3, Z = 2, F(000) = 388, ρ = 1.366 mg/m^{-3}, R_1 = 0.0443, wR_2 = 0.1113, GOF = 1.077, residual electron density between 0.161 and -0.246 eÅ^{-3}. CCDC-1029825.

Borebt2: $C_{23}H_{19}BF_2N_2S$; Monoclinic, P21/c, a = 11.3993(10) Å, b = 12.7664(9) Å, c = 15.0074(17) Å, α = 90°, β = 117.220(7)°, γ = 90°, V = 1942.1(3) Å^3, Z = 4, F(000) = 840, ρ = 1.383 mg/m^{-3}, R_1 = 0.0520, wR_2 = 0.1249, GOF = 1.025, residual electron density between 0.217 and -0.257 eÅ^{-3}. CCDC-1029826.

Borebt3: $C_{23}H_{20}BF_2N_3S$; Orthorhombic, Pbca, a = 15.8955(3) Å, b = 9.83109(15) Å, c = 26.4038(6) Å, α = 90°, β = 90°, γ = 90°, V = 4126.12(14) Å^3, Z = 8, F(000) = 1744, ρ = 1.350 mg/m^{-3}, R_1 = 0.0407, wR_2 = 0.1076, GOF = 1.023, residual electron density between 0.186 and -0.232 eÅ^{-3}. CCDC-1029827.

Borebt4: $C_{23}H_{20}BF_2N_3S$; Monoclinic, P2(1)/c, a = 12.1191(13) Å, b = 14.1236(14) Å, c = 11.9134(11) Å, α = 90°, β = 100.907(2)°, γ = 90°, V = 2002.3(3) Å^3, Z = 4, F(000) = 872, ρ = 1.391 mg/m^{-3}, R_1 = 0.0480, wR_2 = 0.1341, GOF = 0.948, residual electron density between 0.255 and -0.247 eÅ^{-3}. CCDC-1029828.

Borebt5: $C_{25}H_{24}BF_2N_3S$; Monoclinic, P2(1)/c, a = 13.0949(9) Å, b = 12.1529(6) Å, c = 14.5043(9) Å, α = 90°, β = 104.475(7)°, γ = 90°, V = 2235.0(2) Å^3, Z = 4, F(000) = 936, ρ = 1.329 mg/m^{-3}, R_1 = 0.0542, wR_2 = 0.1351, GOF = 1.022, residual electron density between 0.171 and -0.222 eÅ^{-3}. CCDC-1029829.

Borebt6: $C_{25}H_{25}BF_2N_4S$; Monoclinic, C2/c, a = 20.6963(13) Å, b = 8.5511(6) Å, c = 27.318(2) Å, α = 90°, β = 106.475(7)°, γ = 90°, V = 4636.1(6) Å^3, Z = 8, F(000) = 1936, ρ = 1.325 mg/m^{-3}, R_1 = 0.0530, wR_2 = 0.1254, GOF = 1.016, residual electron density between 0.181 and -0.228 eÅ^{-3}. CCDC-1029830.

Computational details

TD-DFT calculations were performed at the hybrid density functional theory level (B3LYP) with the 6-31G(d,p) basis set, using the Gaussian03 software package. The calculations were made in the gas phase.[9]

Electrochemical Properties.

Cyclic voltammetry were recorded with a CHI 660B electrochemical analyzer using degassed and dried CH_2Cl_2 under an argon atmosphere. The CV cell consisted of a glassy carbon electrode, a Pt wire counter electrode, and a Ag/AgCl reference electrode. All measurements were performed using CH_2Cl_2 solutions of samples with a concentration of 1 mM and 0.1 M Bu_4NBF_4 as a supporting electrolyte with a scan rate of 50 mVs^{-1}. Potentials were determined against a ferrocene/ferrocenyl ion couple (Fc/Fc^+). The frontier orbital energy levels were calculated with the following equation[12]:

$E_{HOMO} = - E_{ox/on\ set} - 4.8$ eV

$E_{LUMO} = - E_{Red/on\ set} - 4.8$ eV

Acknowledgements

We thank the Natural Science Foundation of China (nos. 21301085), the Natural Science Foundation of Shandong Province (ZR2011BQ010), and the Liaocheng University Funds for Young Scientists (31805) for financial support.

Notes and references

[a] Institute of Organic Functional Molecules and Materials, School of Chemistry and Chemical Engineering, and School of Material Science and Engineering, Liaocheng University, 1, Hunan road, Liaocheng, Shandong, P.R. China. Email: chliuzp@163.com; wangxiaoqing@lcu.edu.cn; gongshw@lcu.edu.cn.

[b] School of Pharmacy, Liaocheng University, 1, Hunan road, Liaocheng, Shandong, P.R. China.

[c] Qufu Normal University, Qufu, 273165, Shandong, P.R. China.

Electronic Supplementary Information (ESI) available: Synthesis, ^{1}H, ^{13}C, ^{11}B NMR spectra, absorption and fluorescent spectra of compound **Borebt1-6**. See DOI: 10.1039/b000000x/

1 (a) C. W. Tang, S. A. VanSlyke, *Appl. Phys. Lett.* 1987, **51**, 913; (b) R. H. Friend, R. W. Gymer, A. B. Holmes, J. H. Burroughes, R. N. Marks, C. Taliani, D. D. C. Bradley, D. A. Dos Santos, J. L. Brédas, M. Lögdlund, W. R. Salaneck, *Nature.* 1999, **397**, 121.

2 (a) A. Loudet, K. Burgess, *Chem. Rev.* 2007, **107**, 4891; (b) G. Ulrich, R. Ziessel, A. Harriman, *Angew. Chem. Int. Ed.* 2008, **47**, 1184; (c) D. Frath, J. Massue, G. Ulrich, and R. Ziessel, *Angew. Chem., Int. Ed.*, 2014, **53**, 2290; (d) H. Lu, J. Mack, Y. Yang, Z. Shen, *Chem. Soc. Rev.*, 2014, **43**, 4778.

3 (a) A. Hepp, G. Uirich, R. Schmechel, H. von Seggern, R. Ziessel, Synth. Met., 2004, **146**, 11; (b) D. Zhang, Y. Wen, Y. Xiao, G. Yu, Y. Liu, X. Qian, *Chem. Commun*., 2008, 4777; (c) T. Ozdemir, S. Atilgan, I. Kutuk, L. T. Yildirim, A. Tulek, M. Bayindir, E. U. Akkaya, *Org. Lett.*, 2009, **11**, 2105.

4 Examples for the BODIPY analogues developed from desymmetrized *N*,*N*-bidentate ligands. (a) L. Wu, K. Burgess, *J. Am. Chem. Soc.* 2008, **130**, 4089; (b) Y. Zhou, J. W. Kim, R. Nandhakumar, M. J. Kim, E. Cho, Y. S. Kim, Y. H. Jang, C. Lee, S. Han, K. M. Kim, J.-J. Kim, J. Yoon, *Chem. Common*, 2010, **46**, 6512; (c) J. F. Araneda, W. E. Piers, B. Heyne, M. Parvez, R. McDonald, *Angew. Chem. Int. Ed.* 2011, **50**, 12214; (d) Y. Kubota, H. Hara, S. Tanaka, K. Funabiki, M. Matsui, *Org. Lett.* 2011, **13**, 6544; (e) M. Santra, H. Moon, M.-H. Park, T.-W. Lee, Y. K. Kim, K. H. Ahn, *Chem. Eur. J.* 2012, **18**, 9886; (f) K. Benelhadj, J. Massue, P. Retailleau, G. Ulrich, R. Ziessel, *Org. Lett*. 2013, **15**, 2918; (g) Y.-Y. Wu, Y. Chen, G.-Z. Gou, W.-H. Mu, X.-J. Lv, M.-L. Du, W.-F. Fu, *Org. Lett.*, 2012, **14**, 5226; (h) D. Frath, A. Poirel, G. Ulrich, A. D. Nicola, R. Ziessel, *Chem. Commun*. 2013, **49**, 4908; (i) S. Shimizu, T. Lino, Y. Araki, N. *Chem. Commun*. 2013, **49**, 1621; (j) Y. Ni, W. Zeng, K.-W. Huang, J. Wu, *Chem. Commun*. 2013, **49**, 1217; (k) H. Liu, H. Lu, F. Wu, Z. Li, N. Kobayashi, Z. Shen, *Org. Biomol. Chem*. 2014, **12**, 8223; (l) N. Gao, C. Cheng, H. Yu, E. Hao, S. Wang, J. Wang, Y. Wei, X. Mu, L. Jiao, *Dalton Trans*., 2014, **43**, 7121; (m) X. Wang, H. Liu, J. Cui, Y. Wu, H. Lu, J. Lu, Z. Liu and W. He, *New J. Chem*. 2014, **38**, 1277.

5 (a) H. Lu, Q. Wang, L. Gai, Z. Li, Y. Deng, X. Xiao, G. Lai and Z. Shen, *Chem. –Eur. J*. 2012, **18**, 7852; (b) L. Gai, H. Lu, B. Zou, G. Lai, Z. Shen, Z. Li, *RSC Advances* 2012, **2**, 8840; (c) G.-L. Fu, H. Pan, Y.-H. Zhao, C.-H. Zhao, *Org. Biomol. Chem*. 2011, **9**, 8141. (d) Y. Kubota, J. Uehara, K. Funabiki, M. Ebihara, M. Matsui, *Tetrahedron Lett*. 2010, **51**, 6195; (e) T. T. Vu, S. Badré, C. Dumas-Verdes, J. J.Vachon, C. Julien, P. Audebert, E. Y. Senotrusova, E. Y. Schmidt, B. A. Trofimov, R. B. Pansu, G. Clavier, R. Méallet-Renault, *J. Phys. Chem. C*. 2009, **113**, 11844.

6 (a) Y. Hong, J. W. Y. Lam, B. Z. Tang, *Chem. Commun*. 2009, 4332; (b) Y. Hong, J. W. Y. Lam, B. Z. Tang, *Chem. Soc. Rev*. 2011, **40**, 5361; (c) Z. Zhao, J. W. Y. Lam, B. Z. Tang, Curr. *Org. Chem*. 2010, **14**, 2109.

7 (a) Y. Yang, X. Su, C. N. Carroll, I. Aprahamian, *Chem. Sci*. 2012, **3**, 610; (b) Z. Zhao, Z. Chang, B. He, B. Chen, C. Deng, P. Lu, H. Qiu, B. Z. Tang, *Chem. –Eur. J*. 2013, **19**, 11512; (c) R. Yoshii, A. Hirose, K. Tanaka, Y. Chujo, *Chem. –Eur. J*. 2014, **20**, 8320; d) K. Perumal, J. A. Garg, O. Blacque, R. Saiganesh, S. Kabilan, K. K. Balasubramanian, K. Venkatesan, *Chem. –Asian. J*. 2012, **7**, 2670; (e) L. Quan, Y. Chen, X.-J. Lv, W.-F. Fu, *Chem. –Eur. J*. 2012, **18**, 14599; f) R. Yoshii, A. Nagai, K. Tanaka, Y. Chujo, *Chem. –Eur. J*. 2013, **19**, 4506; (g) Y. Kubota, S. Tanaka, K. Funabiki, M. Matsui, *Org. Lett*. 2012, **14**, 4682.; (h) X. Wang, Y. Wu, Z. Li, Q. Liu, H. Yan, C. Ji, J. Duan, Z. Liu, *Chem. Common.,* 2015, **51**, 784.

8 Gaussian 03, Revision B. 05, M. J. Frisch, G. W. Trucks, H. B. Schlegel, G. E. Scuseria, M. A. Robb, J. R. Cheeseman, J. A. Montgomery, Jr., T. Vreven, K. N. Kudin, J. C. Burant, J. M. Millam, S. S. Iyengar, J. Tomasi, V. Barone, B. Mennucci, M. Cossi, G. Scalmani, N. Rega, G. A. Petersson, H. Nakatsuji, M. Hada, M. Ehara, K. Toyota, R. Fukuda, J. Hasegawa, M. Ishida, T. Nakajima, Y. Honda, O. Kitao, H. Nakai, M. Klene, X. Li, J. E. Knox, H. P. Hratchian, J. B. Cross, V. Bakken, C. Adamo, J. Jaramillo, R. Gomperts, R. E. Stratmann, O. Yazyev, A. J. Austin, R. Cammi, C. Pomelli, J. W. Ochterski, P. Y. Ayala, K. Morokuma, G. A. Voth, P. Salvador, J. J. Dannenberg, V. G. Zakrzewski, S. Dapprich, A. D. Daniels, M. C. Strain, O. Farkas, D. K. Malick, A. D. Rabuck, K. Raghavachari, J. B. Foresman, J. V. Ortiz, Q. Cui, A. G. Baboul, S. Clifford, J. Cioslowski, B. B. Stefanov, G. Liu, A. Liashenko, P. Piskorz, I. Komaromi, R. L. Martin, D. J. Fox, T. Keith, M. A. Al-Laham, C. Y. Peng, A. Nanayakkara, M. Challacombe, P. M. W. Gill, B. Johnson, W. Chen, M. W. Wong, C. Gonzalez, and J. A. Pople, Gaussian, Inc., Pittsburgh, PA, **2003**.

9 X. Chen, Z. Zhang, H. Zhang, S. Han, K. Ye, L. Wang, H. Zhang, and Y. Wang, *J. Mater. Chem. C*, 2014, **2**, 7385.

10 Uchiyama, S.; Matsumura, Y.; de Silva, A. P.; Iwai, K. *Anal. Chem*. 2003, **75**, 5926.

11 Sheldrick, G. M. *SHELX-97*, *Program for the Refinement of Crystal Structures*;University of Göttingen: Göttingen, Germany, 199**7**.

12 V. V. Pavlishchuk, A. W. Addison, *Inorg. Chim. Acta* 2000, **298**, 97.

GRAPHIC ABSTRACT

A series of benzothiazole-enamide-based boron difluoride complexes were demonstrated to possess aggregation-induced emission, tunable, substituent-dependent emission profiles, large Stokes shift and high quantum yield in the solid-state, which were rationalized through X-ray crystal analysis, and electronic structure calculations.